Supporting information

Purely inorganic frameworks based on polyoxometalate cluster with abundant phosphate groups: single-crystal to single-crystal structural transformation and remarkable proton conduction

Shan Zhang, Ying Lu,* Xiu-Wei Sun, Zhuo Li, Tian-Yi Dang, Zhong Zhang, Hong-Rui Tian and Shu-Xia Liu*

Key Laboratory of Polyoxometalate Science of Ministry of Education, Northeast Normal University, Changchun, Jilin, 130024 (China).

*Corresponding author. E-mail address: liusx@nenu.edu.cn, luy968@nenu.edu.cn

Contents

Section S1 Experimental Section

1. Materials:

All the chemicals and reagents including ammonium iron sulfate, Sodium molybdate dihydrate, malic acid, phosphoric acid (85%) were obtained from commercial sources and used without further purification.

2. Instruments:

Elemental analyses (CHN) were conducted on a PerkinElmer 2400 CHN Elemental analyzer. Infrared (IR) spectroscopy was performed in the range of 4000–500 cm^{-1} using the KBr pellet on an Alpha Centaurt FT/IR spectrophotometer. The room temperature powder X-ray diffraction (PXRD) spectra in the range of $2\theta = 5–50°$ were performed on a Siemens D5005 diffractometer with Cu-Kα radiation. X-ray photoelectron spectra (XPS) were collected on Thermo ESCALAB 250 X-ray photoelectron spectrometer. Thermal gravimetric analysis (TGA) was carried out using a Perkin-Elmer TG-7 analyzer in flowing N_2 heated from room temperature to 600 ℃ with a heating rate of 10 ℃/min. The water adsorption and desorption isotherms of the complex **1'** were carried out by ASAP 2020 instrument at 25 ℃. The alternating current (AC) impedance spectroscopy data were obtained using a Solartron SI 1260 Impedance/Gain-Phase Analyzer over the frequency range of 0.1–10^6 Hz and an applied voltage of 200 mV.

3. Synthesis

$H_7\{[Na_2(H_2O)_2Na_4Fe^{III}_4(H_2O)_4(PO_4)][Fe^{II}_{0.5}Mo^{V}_4Mo^{VI}_2(OH)O_{14}(PO_4)_4]_4[Na_2(H_2O)_4Fe^{II}_4(H_2O)_8]\}\cdot 10.36H_2O$ (1).

A mixture of $(NH_4)_2Fe(SO_4)_2\cdot 6H_2O$ (0.667g, 1.7mmol), $Na_2Mo_4\cdot 2H_2O$ (0.726g, 3mmol), malic acid (0.172g, 1.28mmol), H_3PO_4 1mL and 10mL deionized water was stirred at room temperature for 30 min. The final pH = 3.6 adjusted by 2 M NaOH, then sealed in a 25 mL Teflon-lined autoclave and heated at 160 °C for 4 days. After cooling to room temperature slowly, red block crystals suitable for X-ray diffraction were filtered. Vacuum dried for 12 h and yield in 68% based on Mo. Elemental analysis. Calc for **1**: Mo 37.51%; Fe 9.12%; Na 3.00%; P 8.58%; Found: Mo 37.53%; Fe 9.11%; Na 3.01%; P 8.56%; IR (cm^{-1}): 3204 (w), 1625 (s), 1425 (s), 1197 (m), 1045 (w), 1007 (w), 950 (w), 911 (m), 792 (s), 705 (s) , 598 (m), 531 (m).

$H_3\{[Na_2(H_2O)_2Na_4Fe^{III}_4(H_2O)_4(PO_4)][Na_{0.5}(H_2O)Fe^{II}_{0.5}Mo^{V}_4Mo^{VI}_2(OH)O_{14}$-$(PO_4)_4]_4[Fe^{III}_4(H_2O)_8]\}\cdot 12H_2O$ (1').

When **1** was exposed to air for two days, the black block crystal **1'** was obtained. Elemental analysis. Calc for **1'**: Mo 37.34%; Fe 9.07%; Na 2.98%; P 8.54%; Found: Mo 37.35%; Fe 9.06%; Na 2.97%; P 8.55%; IR (cm^{-1}): 3180 (w), 1616 (s), 1416 (s), 1197 (m), 1050 (m), 1004 (m), 950 (w), 912 (m), 788 (s), 703 (m), 589 (m), 532 (m).

4. X-ray crystallography

Single-crystal X-ray diffraction data of compounds **1** and **1'** were collected on a Bruker Smart Apex CCD diffractometer with Mo-Ka radiation (λ = 0.71073 Å) at 100 K. The structures were solved using OLEX2 [1] and refined by full-matrix least-squares method with SHELXL-2015 [2]. During the refinement of compounds **1** and **1'**, the command "omit" was used to omit the weak reflections, and the restraint command "ISOR" was also used to refine the disordered water molecules with ADP problems. All atoms were refined anisotropically. In compound **1**, O3W and O9W were split into O3WA, O3WB and O9WA, O9WB, resulting in their thermal parameters (Ueq) should be close to those of other water molecules. In compound **1'**, O3W also split into O3WA, O3WB. The H atoms on water molecules cannot be fixed because of the weak residual electron peaks, but directly included in the final molecular formula. Crystallographic data for the structures reported in this paper have been deposited in the Cambridge Crystallographic Data Center with CSD numbers 1955851–1955852 for compounds **1** and **1'**. These data can be obtained free of charge from The Cambridge Crystallographic Data Centre *via* www.ccdc.cam.ac.uk/data_request/cif.

[1] O. V. Dolomanov, L. J. Bourhis, R. J. Gildea, J. A. K. Howard, H. Puschmann, *J. Appl. Cryst*., 2009, **42**, 339.

[2] G. M. Sheldrick, *Acta Cryst*., 2008, **A64**, 112.

5. Proton Conductivities Studies

The compacted tablet used for conductivity measurements has a diameter of 0.8 cm and a thickness in the range of 0.06–0.07 cm, which was obtained by pressing crystal powders at 6 Mpa for 1 min. The tablet was sandwiched by two copper-plated electrodes. The changing temperature (25–95 ℃) and relative humidity environments (30 to 98% RH) were controlled by the Memmert HCP108 constant temperature humidity chamber. During the variable temperature/ RH conductivity measurement, samples were equilibrated for at least 2 hours after each step in temperature or 12 hours

for each step in RH. The proton conductivities were calculated using the equation: $\sigma = L / (S \cdot R)$, where L and S are the thickness (cm) and cross-sectional area (cm^2) of the tablet, respectively. The σ is the proton conductivity (S cm^{-1}). The activation energy was calculated from the following Arrhenius equation:

$$\sigma T = \sigma_0 \exp\left(-\frac{E_a}{k_B T}\right)$$

Where σ is the proton conductivity, k_B is the Boltzmann constant, σ_0 is the pre-exponential factor, and T is the temperature.

Section S2 Additional Structural Figures and Characterizations

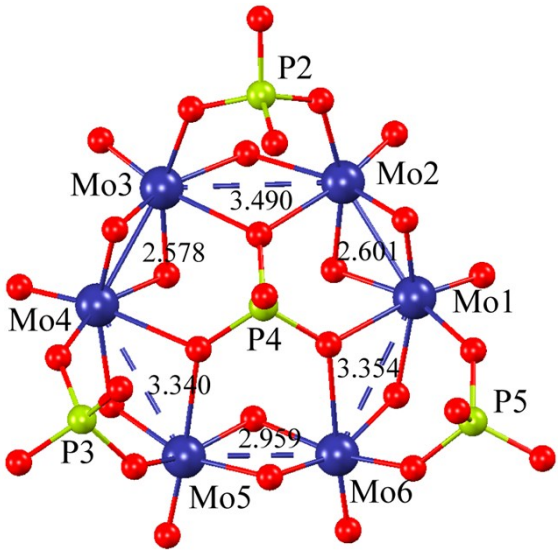

Fig S1 The $\{P_4Mo^{V}_4Mo^{VI}_2\}$ cluster in **1,** and the distances between Mo–Mo bond bonds and Mo···Mo non-bonds.

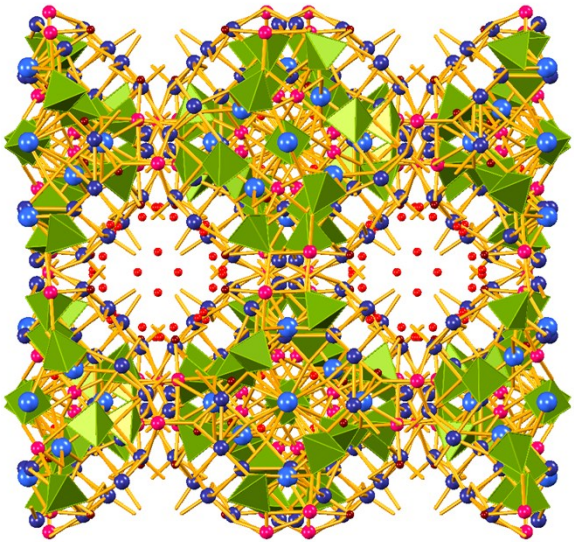

Fig S2 The 3D stacking diagram of compound **1** along the *c*-axis (Mo, indigo; Fe, light pink; Na, light blue; (PO_4), lime tetrahedron; coordination water, dark red; lattice

water, red.)

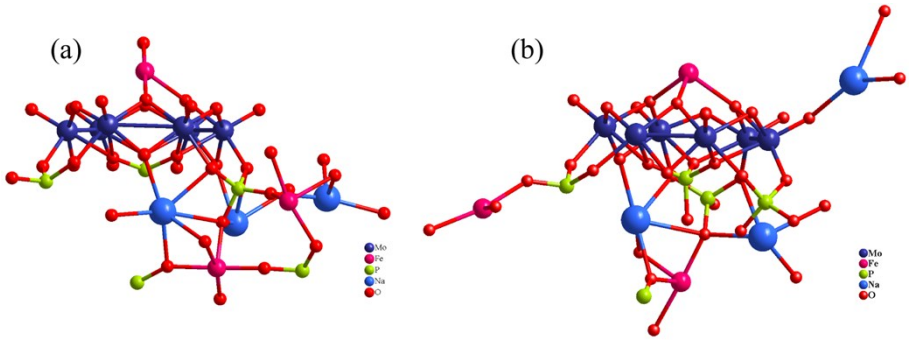

Fig S3 The metal coordination environment of **1** (a); and **1'** (b).

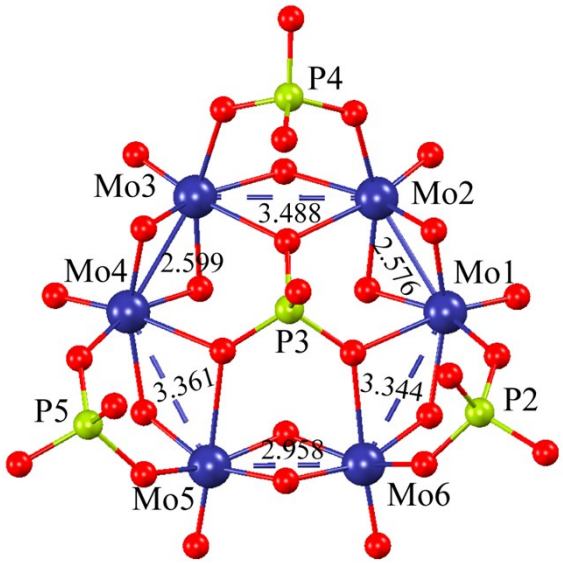

Fig S4 The $\{P_4Mo^{V}_4Mo^{VI}_2\}$ cluster in **1',** and the distances between Mo–Mo bond bonds and Mo···Mo non-bonds.

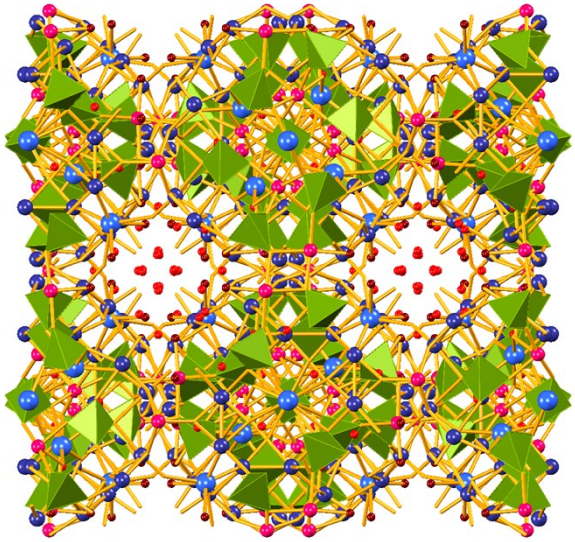

Fig S5 The 3D stacking diagram of compound **1'** along the *c*-axis (Mo, indigo; Fe, light pink; Na, light blue; (PO_4), lime tetrahedron; coordination water, dark red; lattice

water, red.)

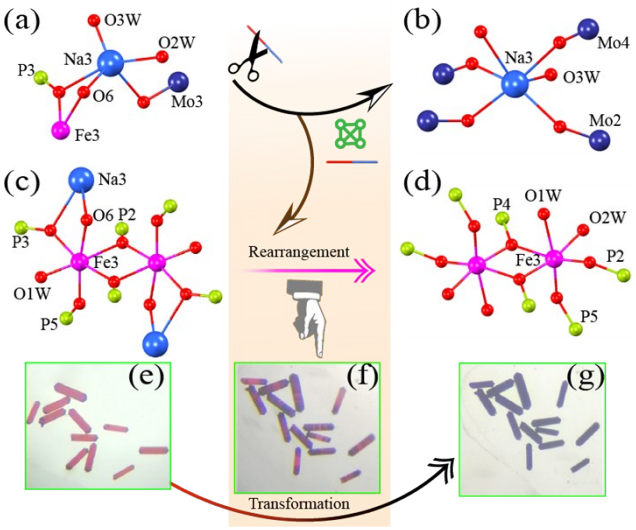

Fig S6 (a) and (c) are the coordination environment diagrams of Na (3) and Fe (3) in **1**, respectively. (b) and (d) are the coordination environment diagrams of Na (3) and Fe (3) in **1'**, respectively. (e–g) changes in crystal color during SCSC transformation were observed under an optical microscope.

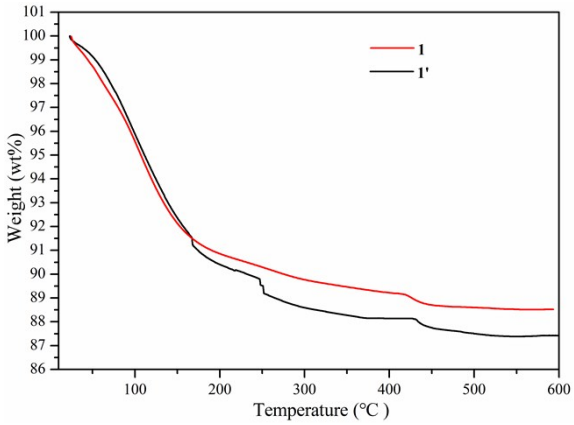

Fig S7 TGA curves of **1** and **1'**.

Thermal stability analysis

During the temperature rises from 25 to 170 ℃, compound **1** and **1'** have a weight loss of 8.41% and 8.75%, respectively. This process is attributed to the loss of 10.36 lattice water molecules and 18 coordination water molecules (calcd. 8.31%) for **1**, and 12 lattice water molecules and 18 coordination water molecules for **1'** (calcd. 8.76%) (Fig S7). Subsequently, the weight decreases slowly with increasing temperature, which is due to partial decomposition of the framework.

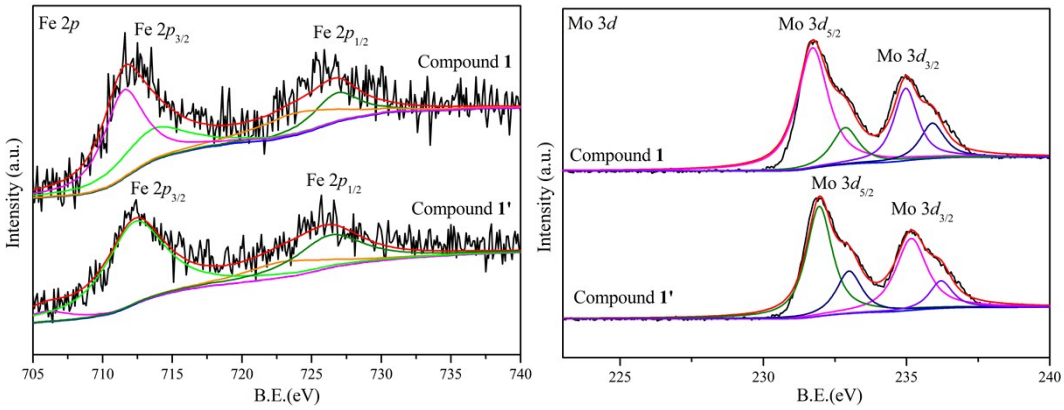

Fig S8 The high-resolution XPS spectrum of the Fe 2p and Mo 3d.

XPS analysis

The high-resolution XPS spectrum of the Fe 2p (Fig. S8) shows two groups of main peaks at binding energies of around 712 and 726 eV, which were attributed to the formation of Fe $2p_{3/2}$ and Fe $2p_{1/2}$ by multiple splitting. Peaks at 711.5, 713.6, 723.8 and 726.8 eV for **1**, and 706.2, 712.3, 723.0, 726.3 eV for **1'** were assigned to the binding energies of Fe^{II} and Fe^{III}.[1] Fig. S8 describes the $3d_{5/2}$ and $3d_{3/2}$ doublet components attributed to Mo 3d in **1** and **1'**. Signal peaks at 231.7 (Mo $3d_{5/2}$) and 235.0 eV (Mo $3d_{3/2}$) for **1**, 231.9 (Mo $3d_{5/2}$) and 235.2 eV (Mo $3d_{3/2}$) for **1'** belong to the Mo^{V}. Meanwhile, binding energies at 232.8 (Mo $3d_{5/2}$) and 236.1 eV (Mo $3d_{3/2}$) for **1**, 232.9 (Mo $3d_{5/2}$) and 236.2 eV (Mo $3d_{3/2}$) for **1'** are attributed to Mo^{VI}, indicating that both compounds contain mixed valence molybdenum.[2]

[1] Z. B. Xiong, B. Peng, F. Zhou, C. Wu, W. Lu, J. Jin, S. F. Ding, *Powder Technology*., 2017, **319**, 19.
[2] L. N. Xiao, C. X. Zhao, X. M. Shi, H. Zhang, W. Wu and X. B. Cui, *CrystEngComm*., 2018, **20**, 969.

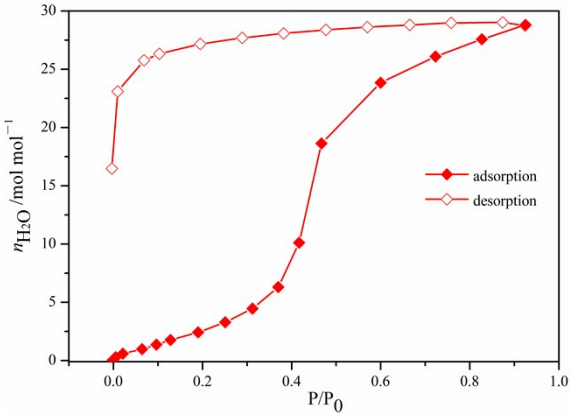

Fig S9 Water adsorption (filled circles) and desorption (open circles) isotherms of **1'** at 25 ℃.

Fig S9 illustrates the stepwise adsorption and desorption processes of **1'** in the P/P_0 range of 0–0.92. With the increase of P/P_0, the amount of water adsorbed gradually

increases, the numbers of water molecules per molecular unit are 18.03 and 28.98 at P/P_0 of 0.46 and 0.92, respectively. The first one corresponds to eighteen coordinated water molecules, while the last one corresponds to lattice water molecules, in agreement with the results of the X-ray diffraction analysis. Desorption isotherm also presents two-step process. The water molecules per molecular unit are 26.31 and 16.53 when P/P_0 reaches 0.10 and 0.00, indicating that even at low pressure there are still a large amount of water molecules that cannot be released.

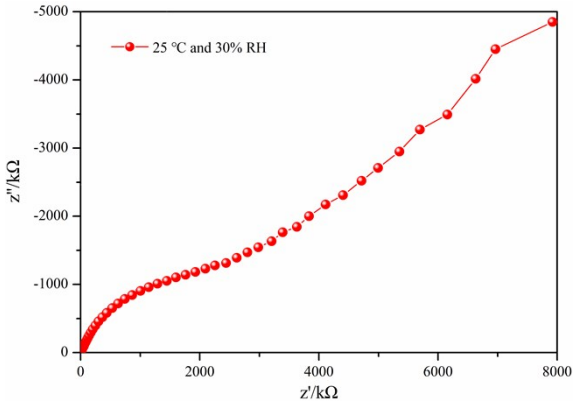

Fig S10 Nyquist plot for **1'** at 25 ℃ and 30% RH.

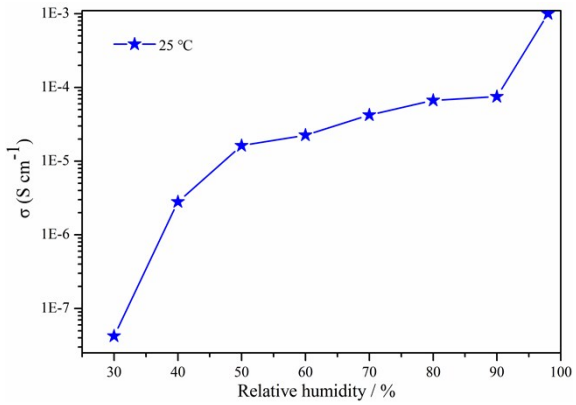

Fig S11 Humidity dependence of conductivities at 25 °C for **1'**.

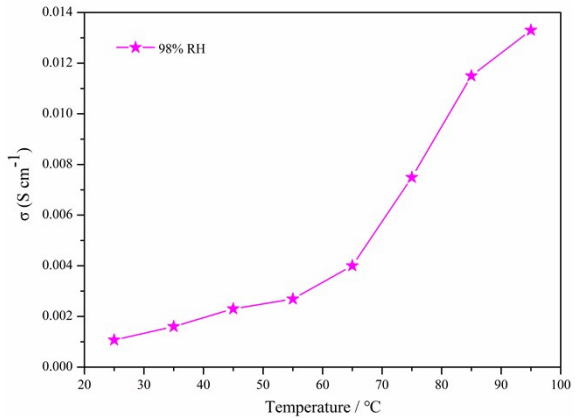

Fig S12 Temperature-dependent conductivities of **1'** under 98% RH.

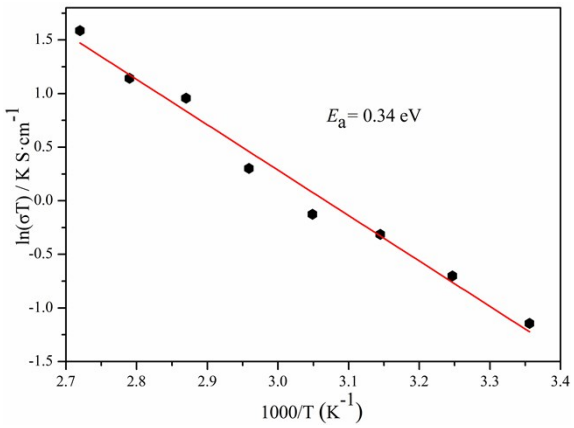

Fig S13 Arrhenius plot of the proton conductivities for **1'** at 98% RH, east-squares fitting is shown as red line.

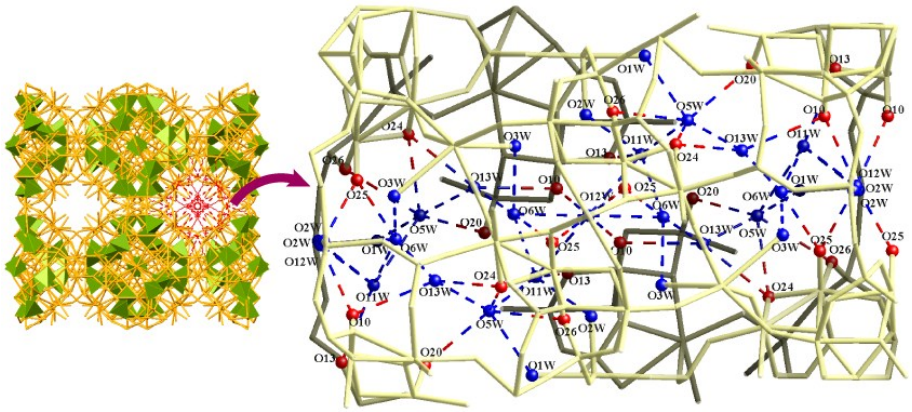

Fig S14 Potentially extensive hydrogen bond networks in 1D channel of **1'**.

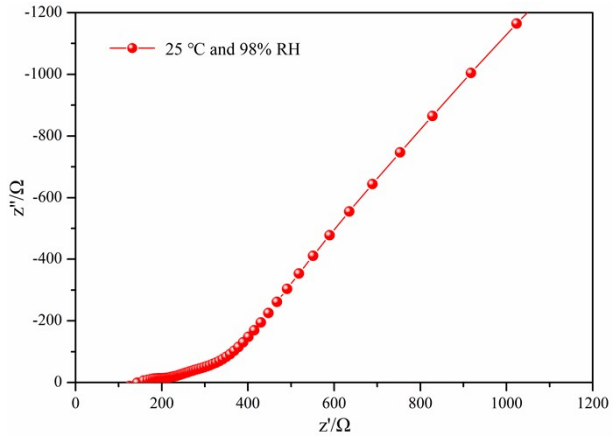

Fig S15 Nyquist plot for **1** at 25 ℃ and 98% RH.

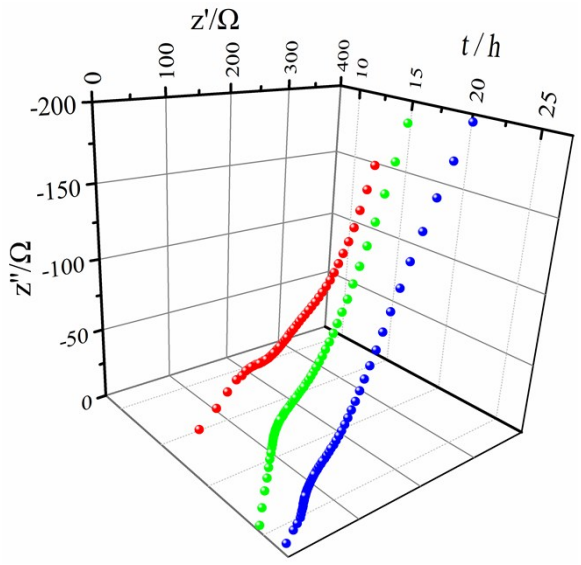

Fig S16 Nyquist plots of **1** with time (12h, red; 18h, green; 24h, blue) at 25 ℃ and 98% RH.

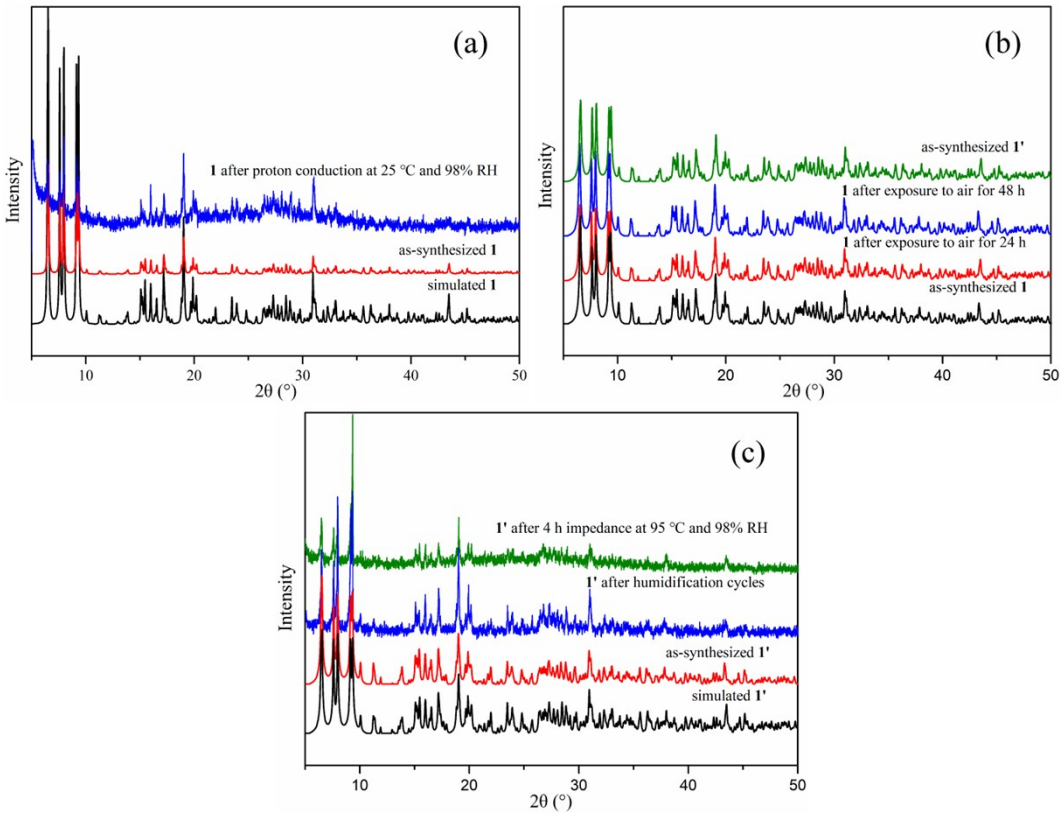

Fig S17 (a) PXRD profiles of single crystal data simulation for **1;** as-synthesized of **1**; after the proton conduction studies of **1**. (b) Time-dependent PXRD profiles of **1** in air. (c) PXRD profiles of single crystal data simulation for **1';** as-synthesized of **1'**; after the proton conduction studies of **1'**.

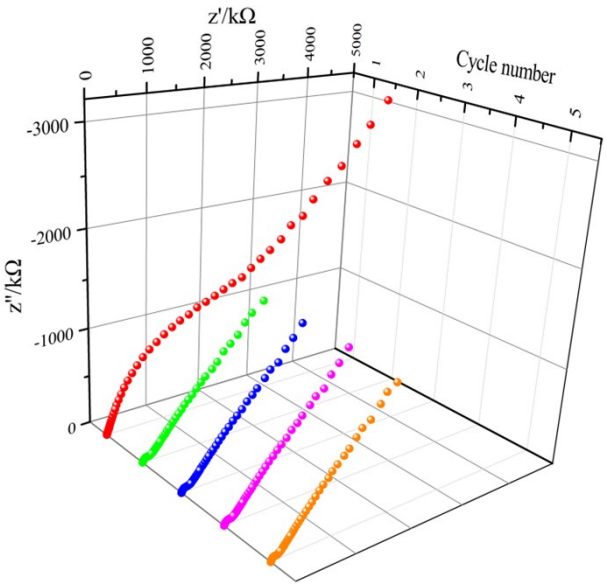

Fig S18 Nyquist plots of four cycles at 25 ℃ and 30% RH for **1'**.

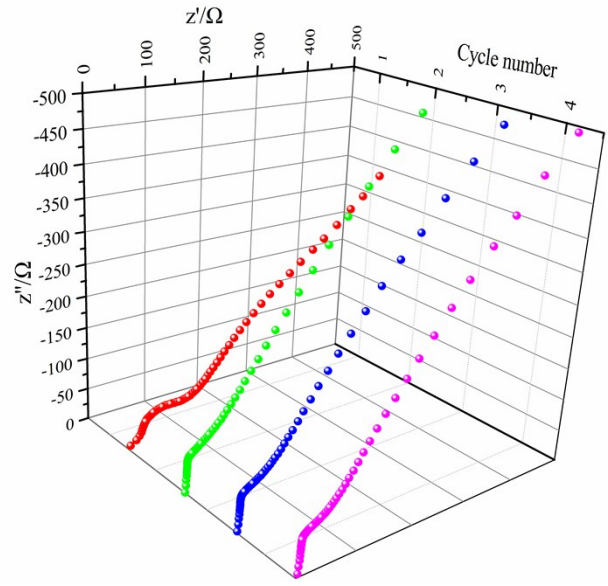

Fig S19 Nyquist plots of four cycles at 25 ℃ and 98% RH for **1'**.

Section S3 Additional Tables

Table S1 X-ray crystallographic data for **1** and **1'**.

Compound	**1**	**1'**
Empirical formula	$Fe_{40}H_{270.72}Mo_{96}Na_{32}O_{625.43}P_{68}$	$Fe_{40}H_{268}Mo_{96}Na_{32}O_{632}P_{68}$
Formula weight	24564.62	24665.88
Temperature (K)	100.0	100.0
Crystal system	Tetragonal	Tetragonal
Space group	$I4_1/acd$	$I4_1/acd$
a (Å)	27.3577(9)	27.3329(12)

b (Å)	27.3577(9)	27.3329(12)
c (Å)	38.0332(12)	37.8621(14)
α (°)	90	90
β (°)	90	90
γ (°)	90	90
Volume (Å^3)	28466(2)	28286(3)
Z	2	2
D_{calc}/gcm^{-3}	2.834	2.865
μ/mm^{-1}	3.369	3.392
F(000)	22895	23000
Reflections collected	79867	73586
Independent reflections	6311 [R_{int} = 0.0683]	6960 [R_{int} = 0.0398]
GOOF	1.083	1.051
Final *R* indexes [I>=2σ (*I*)][ab]	R_1 = 0.0388, wR_2 = 0.0968	R_1 = 0.0317, wR_2 = 0.0897
Final *R* indexes [all data]	R_1 = 0.0574, wR_2 = 1.064	R_1 = 0.0420, wR_2 = 0.0962

[a]$R_1 = \Sigma||F_o|-|F_c||/\Sigma|F_o|$; [b]$wR_2 = \{\Sigma [w(F_o^2-F_c^2)^2]/\Sigma [w(F_o^2)^2]\}^{1/2}$

Table S2 Distances between non-hydrogen atoms in hydrogen bonding that might be constructed by two discrete water clusters in compound **1** (H not directly observed).

Atoms involved	Length (Å)	Atoms involved	Length (Å)
O6W···O10W	2.690	O7W···O9W	3.125
O7W···O5W	3.073		

Table S3 BVS for the iron and molybdenum atoms in **1**.

Atom	BVS result
Fe1	3.192
Fe2	1.702
Fe3	2.305
Mo1	5.25
Mo2	5.267
Mo3	5.22
Mo4	5.289
Mo5	6.067
Mo6	6.075

Table S4 Distances between non-hydrogen atoms in hydrogen bond networks that might be constructed by 1D infinite water tape in compound **1'** (H not directly observed).

Atoms involved	Length (Å)	Atoms involved	Length (Å)
O6W···O13W	2.238	O6W···O11W	2.864
O5W···O13W	2.410	O12W···O11W	3.190
O6W···O12W	2.656	O11W···O5W	3.199

Table S5 BVS for the iron and molybdenum atoms in **1'**.

Atom	BVS result
Fe1	3.248
Fe2	1.699
Fe3	2.674
Mo1	5.266
Mo2	5.192
Mo3	5.229
Mo4	5.272
Mo5	6.048
Mo6	6.04

Table S6 The ratios of Fe^{II}/Fe_{total}, Fe^{III}/Fe_{total}, and Mo^{V}/Mo_{total}, Mo^{VI}/Mo_{total} of **1** and **1'**.

	Compound **1**	Compound **1'**
Fe^{II}/Mo_{total}	60%	20%
Fe^{III}/Mo_{total}	40%	80%
Mo^{V}/Mo_{total}	66.7%	66.7%
Mo^{VI}/Mo_{total}	33.3%	33.3%

Table S7 Compare proton conductivity (at 25℃, 98% RH) of **1'** with other crystalline proton conductor materials under similar conditions.

Compound	Conduction (Temp., RH)	Conductivity (S cm^{-1})	Ref
$\{Na_7[(nBu)_4N]_{17}\}[Zn(P_3Mo_6O_{29})_2]_2\cdot x$ guest solvent molecules	25℃, 100% RH	3.63×10^{-3}	1
$[Co(4,4'\text{-bipy})(H_2O)_4][Co(4,4'\text{-bipyH})_2(H_2O)_4]\cdot 2\text{-}(H_3bmt)\cdot 6H_2O$	25℃, 98% RH	2.02×10^{-3}	2
$H_3\{[Na_2(H_2O)_2Na_4Fe^{III}_4(H_2O)_4(PO_4)]\text{-}[Na_{0.5}\text{-}(H_2O)Fe^{II}_{0.5}Mo^{V}_4Mo^{VI}_2(OH)O_{14}(PO_4)_4]_4\text{-}[Fe^{III}_4(H_2O)_8]\}\cdot 12H_2O$	25℃, 98% RH	1.07×10^{-3}	This work
$[Ni(4,4'\text{-bipyH})_2(H_2O)_4]\cdot 2(H_4bmt)\cdot 9H_2O$	25℃, 98% RH	9.74×10^{-4}	2
$\{[Co_3(DMPhIDC)_2(H_2O)_6]\cdot 2H_2O\}n$	30℃, 98% RH	8.91×10^{-4}	3

$[\{Cu(pip)_2\}_2\{La_{29}Ge_{10}W_{106}O_{406}(OH)_4(H_2O)_{28}\}]^{49-}$	30℃, 98% RH	6.2×10^{-4}	4
$[PMo_{11.04}V_{0.96}O_{40}][C_3H_5N_2]4\cdot H_2O$	50℃, 98% RH	4.45×10^{-4}	5
$H[Ce(H_2O)_4]_2[MnV_{13}O_{38}]\cdot 9NMP\cdot 17H_2O$	25℃, 95% RH	2.66×10^{-4}	6
$H[La(H_2O)_4]_2[MnV_{13}O_{38}]\cdot 9NMP\cdot 17H_2O$	25℃, 95% RH	2.17×10^{-4}	6
$(CH_3NH_3)_2Ag_4Sn_3S_8$	32℃, 99% RH	1.03×10^{-4}	3
$\{[Co_3(DMPhIDC)_2(H_2O)_6]\cdot 2H_2O\}n$	30℃, 98% RH	9×10^{-5}	3
$Na_4K_4(H_2pip)_6(H_2O)_{10}\{Ln_{10}(\mu_3\text{-}OH)_2(H_2O)_{10}$-$[\alpha(1,8)\text{-}GeW_{10}O_{38}]_2[\beta(4,11)GeW_{10}O_{38}]_2\}\cdot 29H_2O$	30℃, 98% RH	4.68×10^{-5}	7
$\{[Cu(H_2bpdc)(H_2O)_{2.5}]_2[SiW_{12}O_{40}]\}\cdot 10H_2O$	25℃, 98% RH	2.36×10^{-5}	8
$(Me_2NH_2)[Eu(L)]$	30℃, 98% RH	2.17×10^{-5}	9
$[Cu(p\text{-}IPhHIDC)]_n$	25℃, 98% RH	1.48×10^{-5}	10
$[Ba(o\text{-}CbPhH_2IDC)(H_2O)_4]_n$	30℃, 98% RH	1.17×10^{-5}	11
$\{Na[Cd(MIDC)]\}n$	25℃, 98% RH	1.13×10^{-5}	12
$[PMo_{12}O_{40}][C_7H_7N_2]_3\cdot 2H_2O$	50℃, 98% RH	6.87×10^{-6}	5
$[Cu_3(\mu_3\text{-}OH)(H_2O)_3(atz)_3]_3[P_2W_{18}O_{62}]\cdot 14H_2O$	25℃, 97% RH	4.4×10^{-6}	13
$(TMA)_{14}H_2[Ce^{III}(H_2O)_6]\{[Ce^{IV}_7Ce^{III}_3O_6(OH)_6(CO_3)$-$(H_2O)_{11}][(P_2W_{16}O_{59})]_3\}\cdot 41H_2O$	30℃, 98% RH	1.95×10^{-7}	14
$Cu_6(Trz)_{10}(H_2O)_4[H_2SiW_{12}O_{40}]\cdot 8H_2O$	45℃, 95% RH	5.4×10^{-8}	15

Table S8 Compare proton conductivity (at 95℃, 98% RH) of **1'** with other crystalline proton conductor materials under similar conditions.

Compound	Conduction (Temp., RH)	Conductivity (S cm^{-1})	Ref
$H_{14}[Na_6(H_2O)_{12}]_4[K_{42}Ge_8W_{72}O_{272}(H_2O)_{60}]$	85℃, 98% RH	6.8×10^{-2}	16
$\{[Na(NO_3)(H_2O)]_4[Al_{16}(OH)_{24}(H_2O)_8(P_8W_{48}O_{184})]\}^{16-}$	85℃, 98% RH	4.5×10^{-2}	17
$[Fe^{III}_6(\mu\text{-}O)L_4Cl_6]^{2-}$	85℃, 98% RH	2.84×10^{-2}	18
$H_3\{[Na_2(H_2O)_2Na_4Fe^{III}_4(H_2O)_4(PO_4)][Na_{0.5}(H_2O)Fe^{II}_{0.5}$ $Mo^{V}_4Mo^{VI}_2(OH)O_{14}(PO_4)_4]_4[Fe^{III}_4(H_2O)_8]\}\cdot 12H_2O$	95℃, 98% RH	1.33×10^{-2}	This work
$[Ln_3(H_2O)_{22}][P_2W_{15}Ta_3O_{62}]\cdot nH_2O$ (Ln = Nd)	95℃, 98% RH	9.88×10^{-3}	19
$[Co(4,4'\text{-bipy})(H_2O)_4][Co(4,4'\text{-bipyH})_2(H_2O)_4]\cdot$-$2(H_3bmt)\cdot 6H_2O$	85℃, 98% RH	9.87×10^{-3}	2
$[Ln_3(H_2O)_{22}][P_2W_{15}Ta_3O_{62}]\cdot nH_2O$ (Ln = Pr)	95℃, 98% RH	8.85×10^{-3}	19
$[\{Cu(pip)_2\}_2\{La_{29}Ge_{10}W_{106}O_{406}(OH)_4(H_2O)_{28}\}]^{49-}$	85℃, 98% RH	5.3×10^{-3}	12
$H_3[(CH_3)_4N]_{14}[NaSm(PW_{11}O_{39})_3]\cdot 18H_2O$	85℃, 98% RH	4.7×10^{-3}	20
$[Sm(H_2O)_5(gly)_2][Al(OH)_6Mo_6O_{18}]\cdot 10H_2O$	80℃, 95% RH	4.53×10^{-3}	21
$(Me_2NH_2)[Eu(L)]$	100℃,98% RH	3.76×10^{-3}	9
$(TMA)_{14}H_2[Ce^{III}(H_2O)_6]\{[Ce^{IV}_7Ce^{III}_3O_6(OH)_6(CO_3)$-	100℃, 98% RH	2.65×10^{-3}	22

$(H_2O)_{11}][(P_2W_{16}O_{59})]_3\}\cdot 41H_2O$			
$\{[Cu(H_2bpdc)(H_2O)_{2.5}]_2[SiW_{12}O_{40}]\}\cdot 10H_2O$	100℃, 98% RH	1.77×10^{-3}	8
$[Cu(p\text{-}IPhHIDC)]_n$	100℃ ,98% RH	1.51×10^{-3}	10
$[Cu_2(Htzehp)2(4,4'\text{-bipy})]\cdot 3H2O$ (along [100] direction)	80℃, 95% RH	1.43×10^{-3}	23
$\{[Cu(H_2bpdc)(H_2O)_2Cl_{0.5}]_2[PW_{12}O_{40}]\}\cdot 10H_2O$	100℃, 98% RH	1.40×10^{-3}	8
$[Ba(o\text{-}CbPhH_2IDC)(H_2O)_4]_n$	100℃, 98% RH	1.36×10^{-3}	11
{Na[Cd(MIDC)]}n	100℃, 98% RH	1.04×10^{-3}	12
$[Cu_2(H_2O)_2(L1)_3][PMo^{VI}_{11}Mo^{V}O_{40}]$	65℃, 95% RH	2.8×10^{-4}	24
$(TMA)_{14}H_2[Ce^{III}(H_2O)_6]\{[Ce^{IV}_7Ce^{III}_3O_6(OH)_6(CO_3)\text{-}(H_2O)_{11}][(P_2W_{16}O_{59})]_3\}$	100℃, 75% RH	2.65×10^{-4}	14
$(H_2L2)_{0.5}[(Cu^{I}L2)_2(PMo_{12}O_{40})]\cdot H_2O$	65℃, 95% RH	1.9×10^{-4}	24
$Cu_6(Trz)_{10}(H_2O)_4[H_2SiW_{12}O_{40}]\cdot 8H_2O$	95℃,95% RH	1.84×10^{-6}	15

1 X. L. Cao, S. L. Xie, S. L. Li, L. Z. Dong, J. Liu, X. X. Liu, W. B. Wang, Z. M. Su, W. Guan, and Y. Q. Lan, *Chem. Eur. J.,* 2018, **24**, 2365.

2 L. Feng, Z. Q. Pan, H. Zhou, M. Zhou and H. B. Hou, *Dalton Trans.,* 2019, DOI: 10.1039/C9DT02960E.

3 J. X. Wang, Y. D. Wang, M. J. Wei, H. Q. Tan, Y. H. Wang, H. Y. Zang and Y. G. Li, *Inorg. Chem. Front.,* 2018, **5**, 1213.

4 Z. Li, X. X. Li, T. Yang, Z. W. Cai, S. T. Zheng, *Angew. Chem*., 2017, **129**, 2708 – 2713; *Angew. Chem. Int. Ed*. 2017, **56**, 2664.

5 R. L. Liu, Y. R. Liu, S.H. Yu, C. L. Yang, Z. F. Li, and G. Li, *ACS Appl. Mater. Interfaces.,* 2019, **11**, 1713.

6 H. B. Luo, M. Wang, J. Zhang, Z. F. Tian, Y. Zou, and X. M. Ren, *ACS Appl. Mater. Interfaces.,* 2018, **10**, 2619.

7 Y. Hao, L. Zhong, H. H. Li and S. T. Zheng, *Cryst. Growth Des.,* 2019, **19**, 1329.

8 H. Yang, X. Y. Duan, J. J. Lai, and M. L. Wei, *Inorg. Chem.,* 2019, **58**, 1020.

9 Y. S. Wei, X. P. Hu, Z. Han, X. Y. Dong, S. Q. Zang, and T. C. W. Mak, J. Am. Chem. Soc., 2017, **139**, 3505.

10 Z. B. Sun, S. H. Yu, L. L. Zhao, J. F. Wang, Z. F. Li, G. Li, *Chem. Eur. J.,* 2018, **24**, 10829.

11 K. M. Guo, L. L. Zhao, S. H. Yu, W. Y. Zhou, Z. F. Li, and G. Li, *Inorg. Chem.,* 2018, **57**, 7104.

12 K. Lu, A. L. Pelaez, L. C. Wu, Y. Cao, C. H. Zhu, and H. Fu, *Inorg. Chem.,* 2019, **58**, 1794.

13 Y. Q. Jiao, H. Y. Zang, X. L. Wang, E. L. Zhou, B. Q. Song, C. G. Wang, K. Z. Shao, Z. M. Su, *Chem. Commun*., 2015, **51**, 11313.

14 En. L. Zhou, C. Qin, P. Huang, X. L. Wang, W. C. Chen, K. Z. Shao, and Z. M. Su, *Chem. Eur. J.,* 2015, **21**, 11894.

15 Q. Gao, X. L. Wang, J. Xu, X. H. Bu, *Chem. Eur. J.,* 2016, ***22***, 9082.

16 Z. Li, L. D. Lin, H. Yu, X. X. Li, and S. T. Zheng, *Angew. Chem. Int. Ed*., 2018, **57**, 15777.

17 P. Yang, M. Alsufyani, A. H. Emwas, C. Q. Chen, and N. M. Khashab, *Angew. Chem*., 2018, **130**, 13230.

18 L. D. Lin, Z. Li, D. Zhao, J. H. Liu, X. X. Li and S. T. Zheng, *Chem. Commun*., 2019, **55**, 10729.

19 Q. P. Peng, S. J. Li, R. Y. Wang, S. S. Xia, L. H. Xie, J. X. Zhai, J. Zhang, Q. Y. Zhao and X. N. Chen, *Dalton Trans.,* 2017, **46**, 4157.
20 Z. Li, L. D. Lin, D. Zhao, Y. Q. Sun, and S. T. Zheng, *Eur. J. Inorg. Chem.,* 2019, 437.
21 J. Miao, Y. W. Liu, Q. Tang, D. F. He, G. C. Yang, Z. Shi, S. X. Liu, Q. Y. Wu, *Dalton Trans*., 2014, **43**, 14749.
22 P. T. Ma, R. Wan, Y. Y. Wang, F. Hu, D. D. Zhang, J. Y. Niu, and J. P. Wang, *Inorg. Chem.,* 2016, **55**, 918.
23 R. Li, S. H. Wang, X. X. Chen, J. Lu, Z. H. Fu, Y. Li, G. Xu, F. K. Zheng, and G. C. Guo, *Chem. Mater.,* 2017, **29**, 2321.
24 P. T. Ma, R. Wan, Y. Y. Wang, F. Hu, D. D. Zhang, J. Y. Niu, J. P. Wang, *Inorg. Chem*., 2016, **55**, 918.

Table S9 The O···O distances between 1D infinite water tape and the inner surface of the 1D channel, which may form extensive hydrogen bond network in compound **1'** (H not directly observed).

Atoms involved	Length (Å)	Atoms involved	Length (Å)
O25···O6W	2.691	O13···O11W	2.959
O25···O12W	2.803	O24···O13W	3.010
O3W···O6W	2.843	O24···O5W	3.022
O2W···O11W	2.871	O20···O5W	3.047
O10···O12W	2.874	O26···O5W	3.123
O1W···O5W	2.881	O10···O13W	3.163